CHARACTERIZATION OF THE AMPLIFICATION OF FORCES TO NONSTRUCTURAL COMPONENTS USING RECORDED EARTHQUAKE DATA

Xiang Wang and Tara Hutchinson

Department of Structural Engineering
University of California, San Diego

Abstract

The overall scope of this study is to evaluate the acceleration amplification effects of nonstructural components using recorded earthquake responses of buildings and nonstructural components. Specifically, two separate, yet complementary efforts are undertaken, namely: 1) characterizing nonstructural component amplification effects using a large set of building earthquake responses that are available in the CESMD strong motion database, and 2) identifying the dynamic characteristics of instrumented nonstructural components integrated within a full-scale building shake table test program. Findings from this study are intended to supplement current seismic design provisions of nonstructural systems with evidence obtained from recorded data.

Introduction

Nonstructural components and systems account for 70-80% of the overall investment to a building and are critical to their post-earthquake functionality and survivability (Taghavi and Miranda, 2003; FEMA E-74, 2012). In this regard, seismic design recommendations for nonstructural systems have evolved substantially over the past few decades (e.g. ATC 1978, BSSC 1995; BSSC 1998; CEN, 2004; NZS1170.5, 2004). In US practice, design of NCSs is subdivided into acceleration and displacement sensitive systems (ASCE 7, 2016). Design of the former currently relies on a set of simplified equations to determine the seismic design force demand to the NCS, denoted as F_p. The force F_p is primarily a function of the design spectral acceleration, location of the NCS (building height) and component amplification effects bounded within two limit values (Drake and Bachman, 2006):

$$F_p = \frac{0.4 a_p S_{DS} W_p}{R_p / I_p}\left(1 + 2\frac{z}{h}\right) \qquad \text{ASCE 7-16 Equation 13.3-1}$$

$$F_p \le 1.6 S_{DS} W_p I_p \qquad \text{ASCE 7-16 Equation 13.3-2}$$

$$F_p \ge 0.3 S_{DS} W_p I_p \qquad \text{ASCE 7-16 Equation 13.3-3}$$

where W_p is the component operating weight; S_{DS} is the short period spectral acceleration; z is the height in structure of attachment point; h is the total height of structure; a_p is the component amplification factor taken as 1.0 for rigid components and 2.5 for flexible components; I_p and R_p are component importance factor and response modification factor, respectively. It is noted that the supporting structures' acceleration amplification factor is empirically defined as $1+2z/h$. This represents a linear (first mode assumed) distribution of the acceleration amplification over the

height of the building (from 1 at the ground level to 3 at the top of the building), irrespective of the height and lateral force resisting system of individual buildings.

With the objective of assessing the robustness of current code equations (ASCE-7, 2016), the Applied Technology Council recently initiated a multi-phased project, with the second phase particularly focused on undertaking a comprehensive study to investigate the influence of a wide variety of parameters that may affect the estimation of seismic forces to nonstructural components (e.g., building lateral force system, building ductility, component damping, component ductility, and etc.). The project, ATC-120, led to a proposal for an improved equation (NIST, 2018; Lizundia, 2019):

$$\frac{F_p}{W_p} = \mathrm{PGA} \times \left[\frac{\left(\frac{\mathrm{PFA}}{\mathrm{PGA}} \right)}{R_{\mu bldg}} \right] \times \left[\frac{\left(\frac{\mathrm{PCA}}{\mathrm{PFA}} \right)}{R_{pocomp}} \right] \times I_p$$

ATC-120 Equation 4-2
(NIST, 2018)

The above equation assumes that the design force demand to a nonstructural component is determined by two separate amplification effects: a) amplification of the peak ground acceleration (PGA) induced by the supporting structure (terms in the first bracket), and b) amplification of the peak floor acceleration (PFA) induced by the nonstructural component (terms in the second bracket). Major improvements offered by this equation relative to the existing code equation (ASCE-7, 2016) are summarized as follows:

- The PFA/PGA distribution adopts a nonlinear equation as proposed by Alonzo-Rodrigues and Miranda (2016) to address the linear distribution simplification that is generally considered to be conservative (Fathali and Lizundia, 2011).
- Building ductility R_{ubldg} is explicitly considered in the equation to account for the reduced building acceleration responses induced by building ductility (Kazantzi et al., 2018).
- The component amplification factor (denoted as PCA/PFA) incorporates the effects of component inherent damping and component ductility. The PCA/PFA ratio ranges between 1.4 for high-ductility components and 4.0 for elastic components with an assumed damping ratio of 5%.

Complementing the research initiative on the nonstructural seismic design force evaluation led by the ATC-120 project (NIST, 2017 and 2018), the overall scope of the present study aims at exploring the acceleration amplification effects of nonstructural components using recorded earthquake responses of buildings and nonstructural components. This study involves two separate yet complementary efforts are undertaken, namely: 1) characterizing nonstructural component amplification effects using a large set of building earthquake responses that are available in the CESMD strong motion database[1], and 2) identifying the dynamic characteristics of instrumented nonstructural components integrated within a full-scale building shake table test program (Hutchinson et al., 2014; Chen et al., 2016; Pantoli et al., 2016). Findings from the

[1] https://www.strongmotioncenter.org

analysis of these recorded datasets are intended to provide evidence and guidance to current nonstructural seismic design provisions.

Recorded Building Response Analysis

The metadata of all instrumented buildings and the associated earthquake records from the CESMD strong motion database[1] were analyzed to guide the selection of buildings and earthquake records of interest. This database included 581 records for reinforced concrete (RC) buildings and 655 records for steel buildings (as of 6/12/18). The instrumented buildings under each category were further classified based on their story numbers and lateral resisting systems. Using these selection criteria, this study focused on four representative building groups, namely: *RC shear wall*, *RC moment frame*, *steel moment frame*, and *steel braced frame* groups. Moreover, earthquake events with a PGA less than 0.05 g in at least one horizontal direction were excluded due to their very low amplitude. Details of the proposed building groups and the resulting number of associated earthquake records are summarized in Table 1.

Table 1. Summary of building groups and the associated earthquake record per group.

Building lateral system & Earthquake records	**Low-rise (1-4)**	**Mid-rise (5-8)**	**High-rise (>=9)**	**Total Number**
RC shear wall	11	6	10	**27**
# of earthquake records	22	17	24	**63**
RC moment frame	2	6	3	**11**
# of earthquake records	4	14	8	**26**
Steel moment frame	13	7	10	**30**
# of earthquake records	17	13	14	**44**
Steel braced frame	3	3	4	**10**
# of earthquake records	10	4	7	**21**

Individual Building Analysis Procedures

Figure 1 summarizes the analysis procedures for assessing the component amplification effects of individual buildings using recorded floor acceleration responses. The floor response spectra characteristics serve as critical indicators for the evaluation of the seismic demands of nonstructural components. In ***Step 1***, we employ the deterministic-stochastic identification method (Van Overschee and De Moor, 1996) using the recorded acceleration responses of individual buildings to estimate the modal parameters of the buildings (i.e., periods, damping ratios, and mode shapes). In this step, the system input and output involve the building responses at the two horizontal directions. These estimated periods are used to initiate the structural dynamic parameters optimization (in ***Step 2***). In ***Step 2***, we follow the optimization method proposed by Cruz and Miranda (2016 and 2019) to update the building periods and damping ratios associated with individual earthquake events. The proposed modal inclusion criteria allow for enhanced reliability estimation regarding the identified modal parameters of the buildings, particularly the damping ratios. ***Step 3*** involves evaluating the building floor response spectra

[1] https://www.strongmotioncenter.org

using the recorded floor accelerations as well as component amplification factors (denoted as a_p = PCA/PFA), which are obtained by normalizing the floor response spectra against the associated peak floor accelerations. It is noted that the building responses in the two orthogonal horizontal directions are investigated separately, and therefore the building torsional effects are not explicitly considered within the scope of the present study. An example of the resulting component amplification factors of a 5-story hospital building (CSMIP Station #: 23634) and the associated modal characteristics obtained using the proposed analysis procedures are presented in Figure 2.

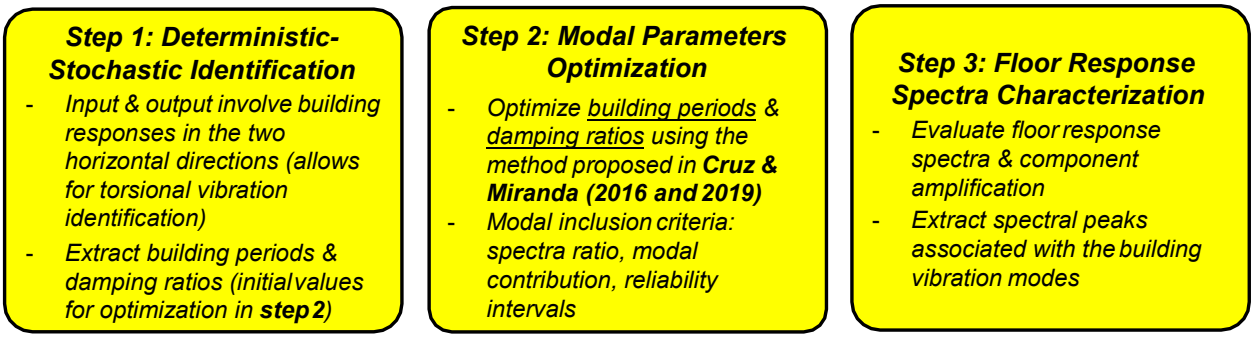

Figure 1. Data analysis procedures for individual buildings.

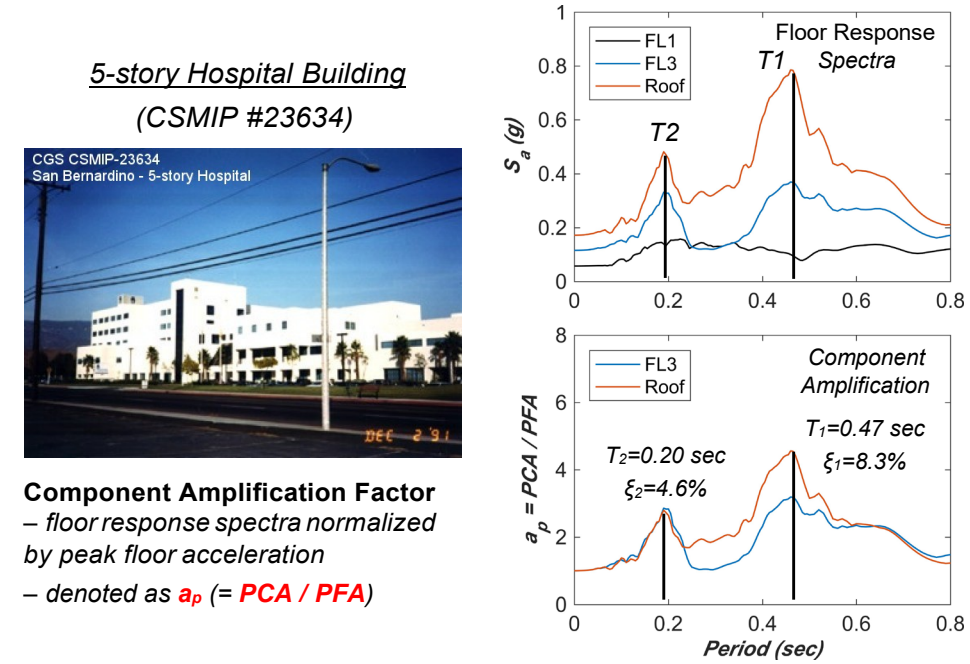

Figure 2. Floor response spectra and component amplification factors a_p of a 5-story hospital building (photograph on left courtesy of CSMIP, Station #: 23634). The floor response spectra represent elastic acceleration spectra with a 5% damping ratio.

Component Amplification of Steel Moment Frame Buildings

The results presented in this section focus on the steel moment frame buildings (see Table 1), whereas those of the remaining building groups will be included in the final project report.

The steel moment frame building group includes a total of 30 buildings subjected to 44 earthquake records with PGA>0.05 g in at least one horizontal direction. With the aim of statistically analyzing the component amplification effects of this building group, the following criteria are adopted in the statistical assessment:

- The analysis of the building responses is decoupled along the two orthogonal directions with no account of the building torsional effects.
- The analysis focuses on the first two building vibration modes (sufficient for low- and mid-rise buildings).
- An upper bound component period is assumed as 0.75 seconds per OSHPD datasets (Watkins et al., 2010). This assumption excludes the fundamental modes of high-rise buildings that are considered unlikely to be tuned with the periods of most nonstructural components.
- The component inherent component damping is assumed to range between 2% ~ 5% (consistent with the range considered by ATC-120).

Following these criteria, the steel moment frame building dataset involves 41 data points for the first modal peaks and 43 data points for the second mode. The component amplification factor (denoted as a_p=PCA/PFA) vs normalized period curves of the roof level associated with the two modes are shown in Figure 3. It is noted that the normalized period represents the ratio of the component period over that of a specific building vibration mode. The component period normalization allows for extraction of the peak component amplification factor associated with individual building vibration modes (within an assumed window of 0.9 ~ 1.1 times the normalized period). Figure 4 presents the relationship between the peak component amplification factors associated with the first and second vibration modes and the identified structural damping ratios related to the corresponding modes. The resulting highly dispersed data points in the plots indicate that the component amplification factors associated with each of the two modes are not well correlated with the damping ratios of the supporting structures. When the assumed component damping ratio reduces from 5% to 2%, comparison of the mean values of the peak component amplification factors reveals that these amplification factors increase by about 50% ~ 60% for both the first and second modes. In addition, the mean peak component amplification factor of the first mode is about 50% larger than that of the second mode.

Figure 5 presents the peak component amplification factors along the height of the buildings. Each data point represents the peak at a specific vertical location (represented by relative height) of an individual building. The color code indicates the building with different stories. It is noted the first mode peaks solely consist of the contribution from the low- and mid-rise buildings. This is due to the fact that all the first mode periods of the high-rise buildings (with 9 stories or more) exceed the upper bound component period of 0.75 second. To facilitate the interpretation of the component amplification distribution along the building height, these data points are grouped into 4 evenly spaced bins according to their relative heights (the center of the representative bins are defined as 0.25, 0.5, 0.75 and 1). Although the bin numbers may not be sufficient for capturing the actual shape associated with the higher modes of mid-rise buildings, a refined binning strategy may not be feasible due to the relative data scarcity in the relative height range between 0.6 and 0.9 (particularly for mid- and high-rise buildings).

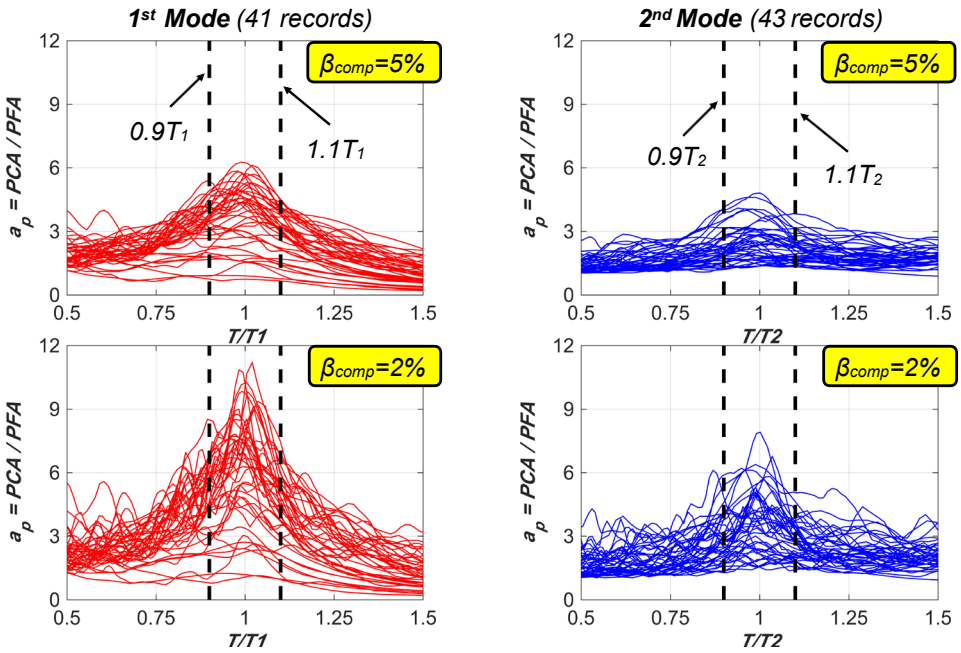

Figure 3. Roof level component amplification factor a_p vs normalized period for: first mode (left), and second mode (right). Upper plots assume a component damping β = 5%, while the lower pair of plots assume β = 2%.

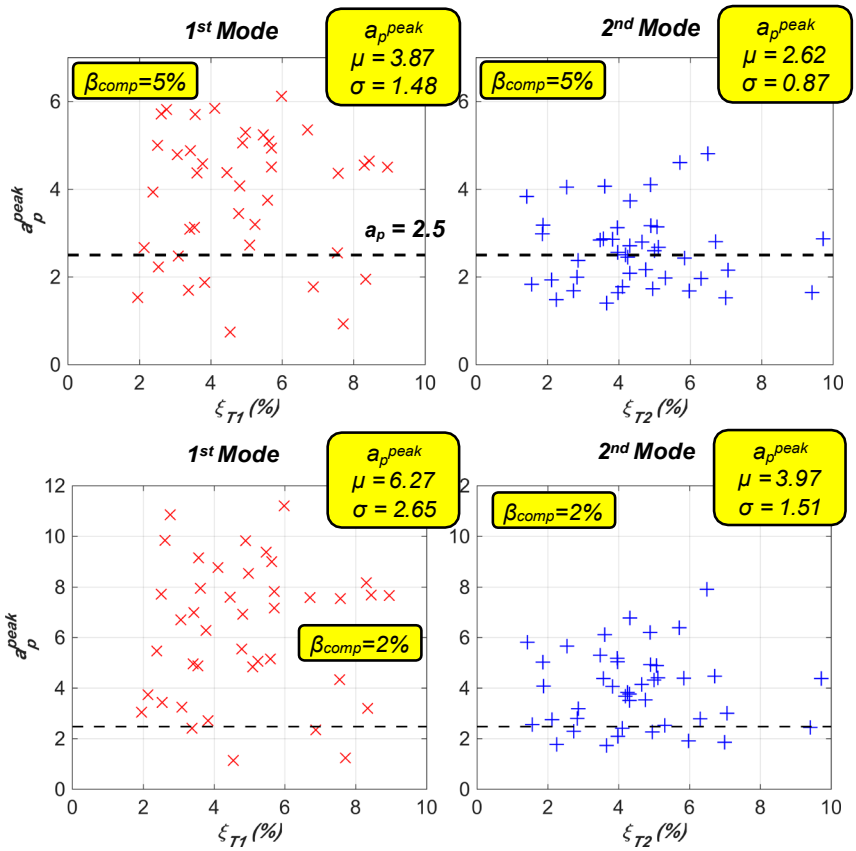

Figure 4. Roof level peak component amplification factor vs structural damping ratio: first mode (left column), and second mode (right column). Upper plots assume a component damping β = 5%, while the lower pair of plots assume β = 2%.

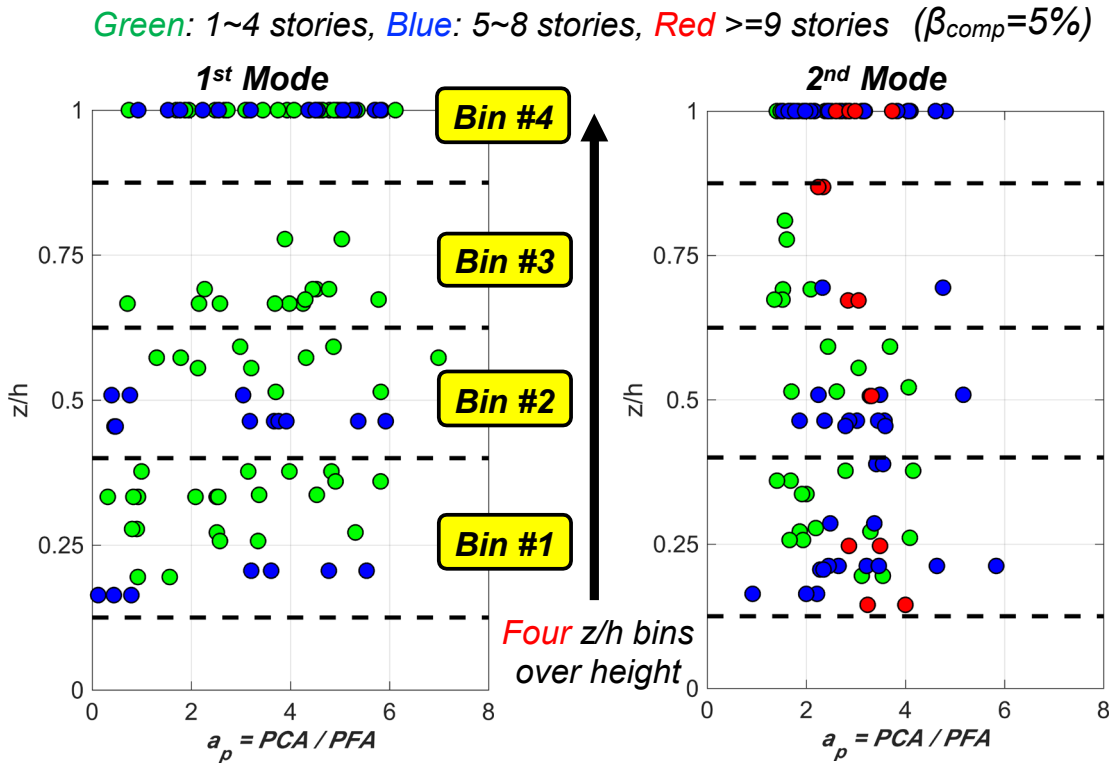

Figure 5. Peak component amplification factor distribution along the height of the buildings (steel moment frame dataset only): first mode (left), and second mode (right).

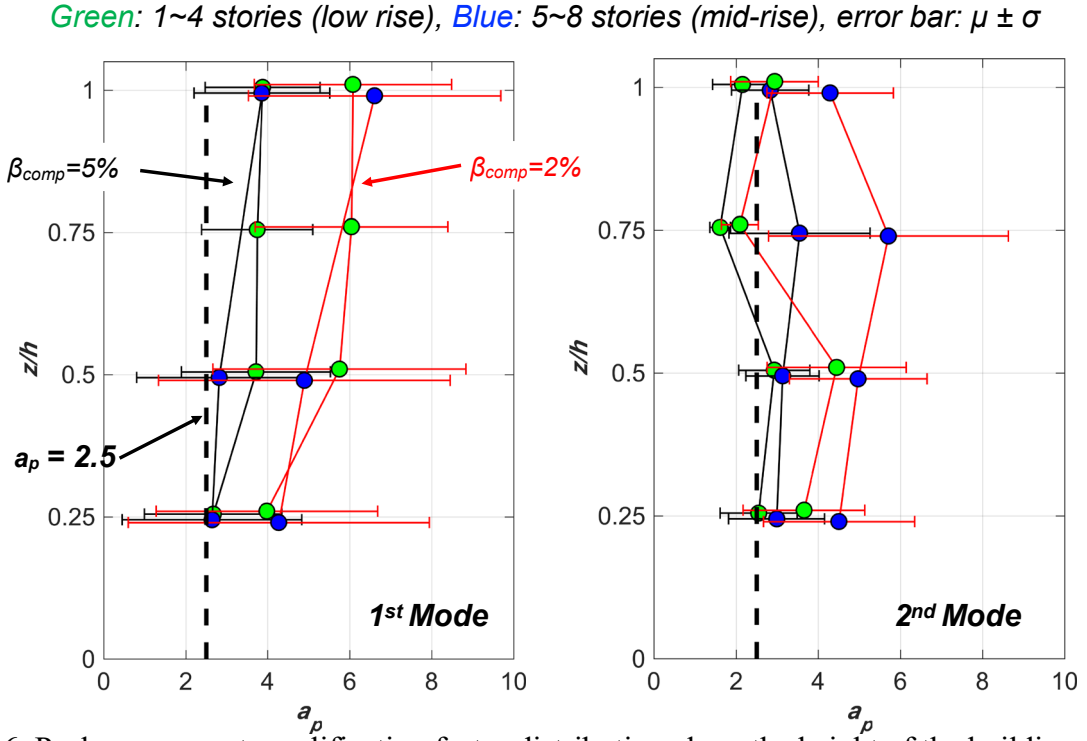

Figure 6. Peak component amplification factor distribution along the height of the buildings: first mode (left), and second mode (right).

Figure 6 summarizes the statistics (i.e., mean and standard deviation) of the vertical distributions of the peak component amplification factors of the low- and mid-rise buildings obtained using the clustered data points. The first mode amplification factors of the low- and mid-rise buildings both increase monotonically and attain the largest values at the roof level. The dispersion of the amplification factors appears comparable at different vertical locations, since the coefficient of variation is 0.5 ~ 0.6 along the height. In contrast, the vertical distribution of the component amplification factors associated with the second mode differs significantly from that of the first mode. For the low-rise buildings, the mean amplification factor reaches the smallest value at the three-quarter building height (z/h = 0.75), which corresponds to the nodal point of the vibration modal shape of the second mode. The differences of the vertical distribution profiles associated with the two modes clearly demonstrate that the component amplification factor is also a function of the specific building mode shape and the relative height.

Recorded Nonstructural Component Response Analysis

Investigating component amplification effects using recorded building responses relies on the evaluation of floor response spectra, which a priori defines nonstructural components as generic linear oscillators given the building floor accelerations. However, the dynamic characteristics (i.e., period and damping ratio) of nonstructural components remains largely unexplored due to the scarcity of measurements during earthquakes, either simulated in the laboratory or obtained in the field (NIST, 2017 and 2018). In a recent experimental program, system-level building shake table tests were conducted at the University of California, San Diego (Chen et al., 2016; Pantoli et al., 2016). These tests provided a unique set of recorded responses of the test building as well as a broad variety of nonstructural components installed within the building (Hutchinson et al., 2014). In this section, the recorded nonstructural seismic responses are analyzed to expand understanding of the dynamic characteristics and the amplification effects of the nonstructural components utilized in this test program under simulated earthquake loading scenarios.

Shake Table Test Program

The test structure was a full-scale five-story reinforced concrete building outfitted with a variety of nonstructural components and systems, including two operable egress systems (elevator and steel stairs), a complete exterior façade system, a broad array of architectural layouts, as well as simulated medical compartments at the upper two floors of the building (Figure 7). In the experimental program, the test building was subjected to a sequence of earthquake tests in two test phases: (i) the building was first tested in base isolated (BI) configuration with seven earthquake tests, and (ii) subsequently in fixed base (FB) configuration with six earthquake tests. It is noted that the earthquake input motions were all applied along the longitudinal axis of the test building using the single-axis shake table.

In the FB test phase, the six earthquake motions were applied with increasing intensity to progressively damage the structure. The first two tests (FB-1 and FB-2) were serviceability earthquake events that the seismic demands of the test structure were sufficiently low (roof peak floor acceleration ~0.4 g). Seismic demands increased moderately in tests FB-3 and FB-4, as the peak acceleration reached ~0.7 g at the roof level. It is noted that test FB-5 is considered as

design event for the test building with the attainment of a peak story drift of ~2.8% at level 2 and a peak floor acceleration of ~1.0 g at the roof, whereas the final test (FB-6) represented a well above design event scenario as the achieved PIDR was as much as 6%. Additional details of the shake table test program, testing protocol, and test results may be found in the technical report series (Chen et al., 2013; Pantoli et al., 2013).

Figure 7. Shake table tests of a five-story reinforced concrete building outfitted with a variety of nonstructural components: test building (left), cooling tower and penthouse of the roof level (top middle left), medical ultrasound imagers of level 4 (bottom middle left), medical equipment of level 4 (top middle right), medical equipment of level 5 (bottom middle right), and computer server at level 3 (right).

Table 2. Description of floor-mounted nonstructural components in the shake table test program.

Nonstructural component	Attachment location	Geometry L x W x H [1] (in)	Operating weight (lb)	Attachment details	Physical observation
Computer server #1 (strong axis shaking)	Floor 3	50 x 30 x 80	3000	(8) M16-25 heavy duty anchors	No damage
Computer server #2 (weak axis shaking)	Floor 3	30 x 50 x 80	3000	(8) M16-25 heavy duty anchors	Incipient screw popping during test FB-4
Ultrasound imager #1	Floor 4	28 x 22 x 58	~300	(4) 1/2" x 3-1/4" expansion anchors	No damage
Ultrasound imager #2	Floor 4	28 x 22 x 58	~300	(4) 1/2" x 3-1/4" expansion anchors	No damage
Medical freezer	Floor 5	30 x 36 x 80	550	(3) 1/2" x 3-1/4" expansion anchors	No damage
Cooling tower [2]	Roof	88 x 108 x 128	6300	(4) snubber spring bearings	Water splashing
Air handling unit	Roof	100 x 58 x 68	1500	(10) 1/2" x 3-1/4" expansion anchors	No damage

[1] H = height, L = length (along shaking direction), W = width (transverse to shaking direction);
[2] Operating weight of the cooling tower consisted of its net weight of 3500 lbs and ~2800 lbs of water during the shake table tests.

Among the nonstructural components and systems installed within the test building, seven pieces of floor-mounted equipment are of interest in this study, since they represented typical acceleration-sensitive components that can be properly simulated as linear oscillators subjected to single-support floor excitations. Detailed descriptions of individual nonstructural components (e.g., geometry, weight, mounting location, attachment details, and etc.) are summarized in Table 2. It is noted that the attachment (or anchor) design of these components conformed to the ASCE-7 (2010 edition) code provisions (ASCE-7, 2010).

Identification of Dynamic Characteristics

The natural periods (or frequencies) and damping ratios of the nonstructural components are identified using the time-domain optimization method with the assumption that they behave as single degree-of-freedom linear oscillators in response to floor excitations. In the optimization algorithm, the objective function is defined as the root mean square error between the simulated response of the oscillator given the measured floor acceleration and the measured response of the nonstructural component (normally at the top of the component). The optimized natural period and damping ratio are obtained by minimizing the objective function (errors between simulated and measured responses). It is noted that the identified damping ratio obtained using this method may be interpreted as an equivalent damping ratio that lumps all possible energy dissipative sources (e.g., friction, contact, yielding). However, the nonstructural components selected for this study did not attain substantial damage during the shake table test sequence, and therefore the hysteretic energy dissipation is not likely to contribute heavily to the damping effects of the components considered in this study.

To demonstrate the effect of nonstructural dynamic characteristics, the two computer servers (see Figure 7 – image on the right) floor-mounted on the slab at level 3 are discussed and compared in detail. Figure 8 shows the time histories of the recorded floor acceleration and the component accelerations of individual units during the first fixed-base test. It is noted that the two servers were identical units but placed in different orientations with respect to the direction of shaking. Whereas Server 1 (strong-axis shaking unit) was oriented with its longitudinal axis was in parallel with the direction of shaking, Server 2 (weak-axis shaking unit) was oriented with its transverse axis in parallel with the direction of shaking (see floor plan layout in Figure 8). Comparison of the acceleration histories indicates that Server 2 underwent substantial amplification relative to the floor excitation, whereas the response of Server 1 remained nearly identical to the floor excitation. In fact, their sharply different dynamic behavior given the identical earthquake excitation results from the distinction of their natural frequencies (or periods) in the direction of shaking. The transfer functions clearly demonstrate that Server 1 was much stiffer than Server 2, since the natural frequency was ~20 Hz for Server 1 and <5 Hz for Server 2.

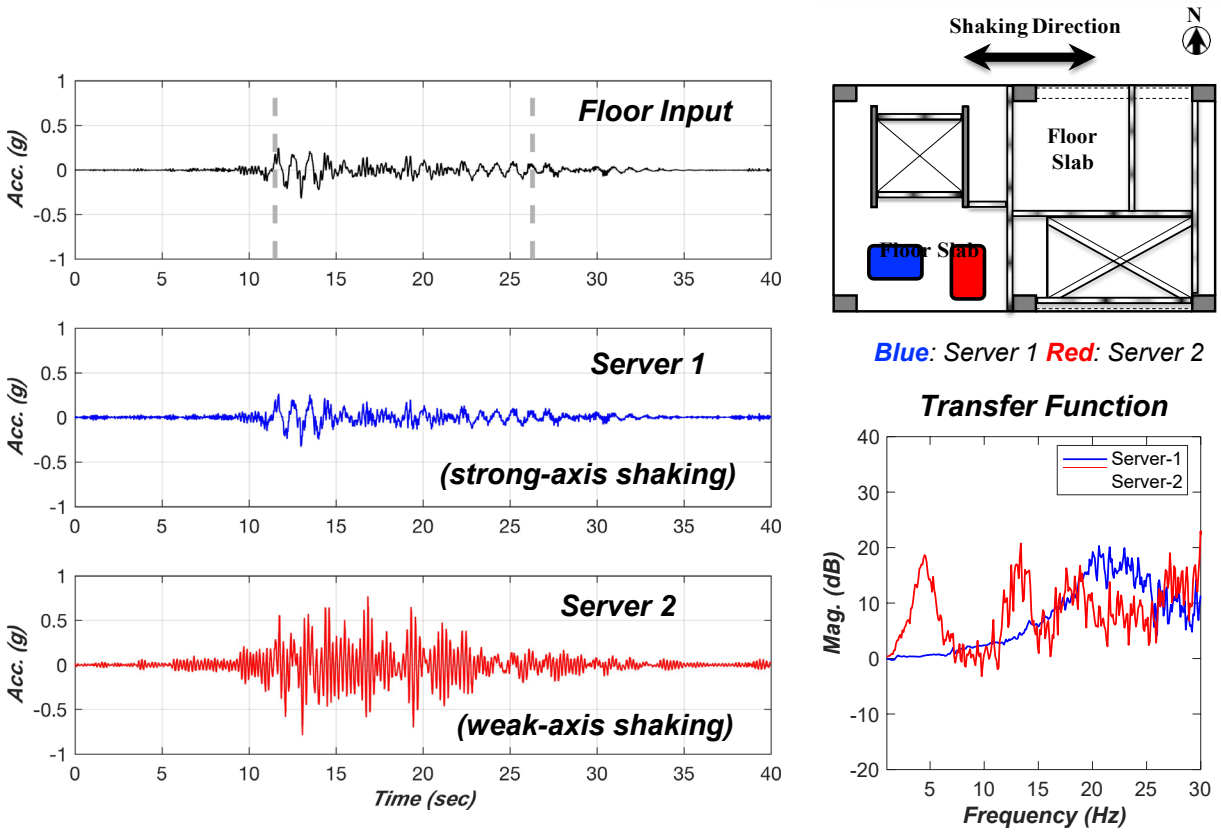

Figure 8. Acceleration time histories of floor 3 and the top of computer servers during the first fixed-base test (left); floor plan layout of level 3 and computer server locations (top right); and the associated transfer functions (bottom right).

The estimated frequencies obtained from the transfer functions provide the initial values for the optimization algorithm. Figure 9 provides the comparison of the recorded and measured component acceleration responses as well as the sensitivity of the identified parameters with respect to the objective function (root mean square error between the measured and simulated responses). Since the minima of the sensitivity curves represent the optimal parameters for the corresponding server unit, the frequency and damping ratio obtained using the optimization method are 25.2 Hz and 9.8% for Server 1 (strong axis shaking) and 4.5 Hz and 6.2% for Server 2 (weak axis shaking). However, it is important to note that both the frequency and damping ratio sensitivity curves for Server 1 appear rather flat in the vicinity of the minima, indicating that the objective function (error) becomes insensitive to the dynamic parameters. In other words, the dynamic parameters obtained from the optimization become less reliable in the case of insignificant component amplification effect. Under such scenarios, the natural frequency of the nonstructural component is determined from the spectral peak of the associated transfer function, whereas its damping ratio is considered as unidentifiable.

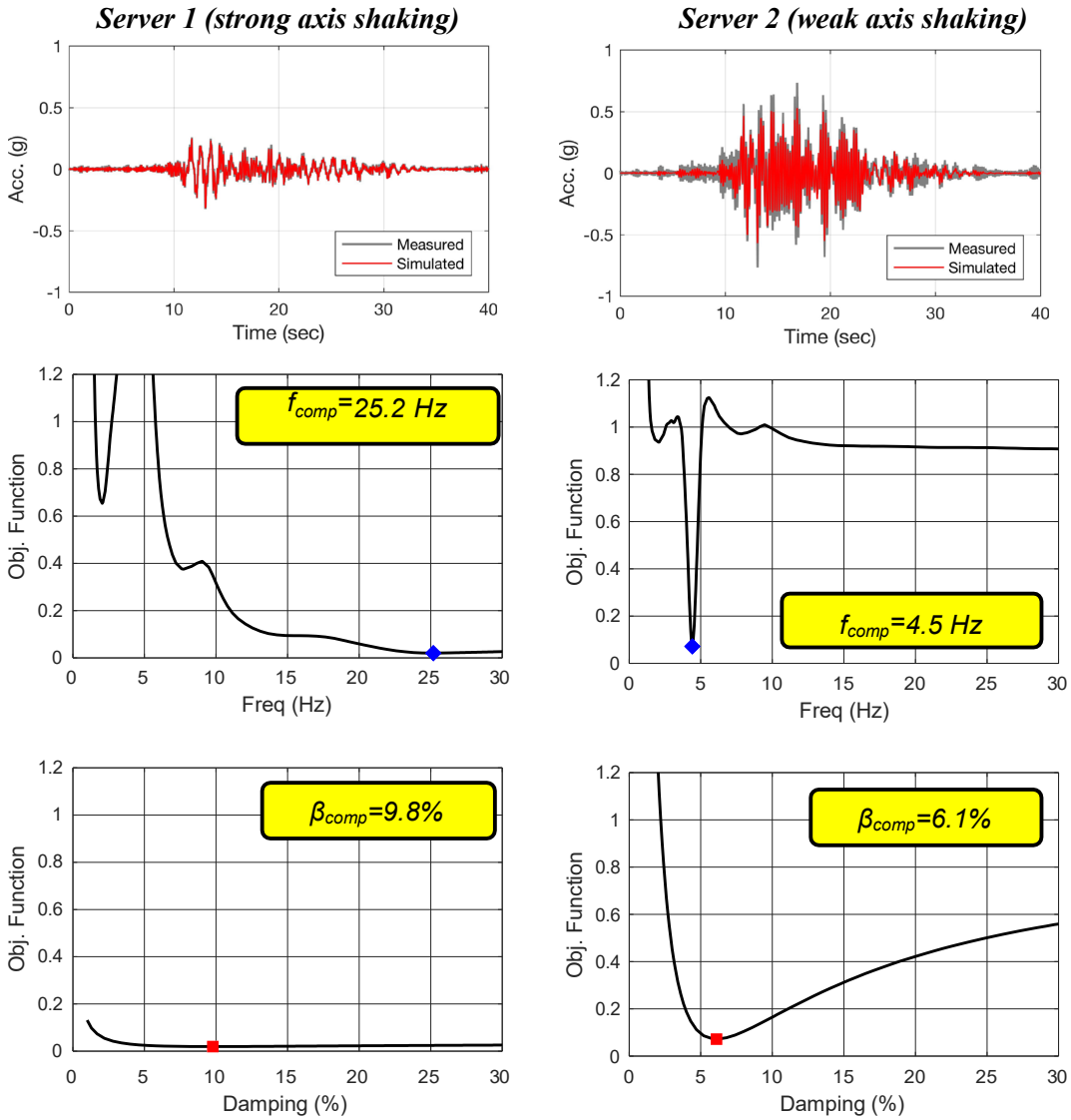

Figure 9. Time-domain dynamic characteristics optimization: measured and simulated component acceleration responses (top); frequency sensitivity curves (middle); and damping ratio sensitivity curves (bottom).

Table 3 summarizes the dynamic characteristics (frequencies and damping ratios) of all nonstructural components considered in this study, as well as the amplification factors as observed from the measured responses during the fixed-base test phase up to design event (FB-1 to FB-5). Results from final test FB-6 are excluded since it represents an extreme event that is normally not considered by the nonstructural design provisions. Among the seven nonstructural components considered in this study, computer server #1 and the air handling unit were rigid components (natural frequencies >20 Hz). The remaining five components were non-rigid components with their natural frequencies range between 4 and 9 Hz. It is noted that the identified damping ratios of these components were between 4.5 and 11, which is larger than the range of 2% and 5% as typically considered in the prior studies (NIST, 2018). Consistent with the ASCE 7 code provisions (ASCE, 2016), the two rigid components (computer server #1 and air handling unit) underwent only very limited acceleration amplification (1.3 as the maximum).

Of the five non-rigid components (with their natural frequencies less than 15 Hz), the measured amplification factors of the computer server #2 and the cooling tower (between 2 and 3) were larger than those of the remaining three components, with values less than 2. The differences in the amplification effects may be attributed to the following two aspects associated with their dynamic characteristics: (1) the natural frequencies of the computer server #2 and the cooling tower were closer to the second mode frequency of the building (~5 Hz during FB-1 but varied at different stages of the test sequence as a result of accumulated structural damage), and (2) the identified damping ratios of the computer server #2 and the cooling tower were moderately smaller than the remaining components.

Table 3. Dynamic characteristics and the component amplification factors of the nonstructural components achieved during the fixed-base tests.

Nonstructural component	Frequency (Hz)	Damping ratio (%)	PCA/PFA
Computer server #1 (strong axis shaking)	22~25	unidentifiable	1.0~1.3
Computer server #2 (weak axis shaking)	4.1~4.6	6.2~7.5	2.0~3.2
Ultrasound imager #1	5.6~7.2	8.5~11.3	1.1~1.6
Ultrasound imager #2	6.5~8.0	7.3~10.8	1.2~1.8
Medical freezer	7.7~9.1	7.1~10.5	1.2~1.5
Cooling tower	4.8~5.6	4.5~5.8	1.9~2.8
Air handling unit	20~22	unidentifiable	1.0

Conclusions and Future Work

With the overall scope of exploring the acceleration amplification effects of nonstructural components using recorded earthquake responses of buildings and nonstructural components. this study focuses on two separate yet complementary tasks: a) characterizing the component amplification effects using a large set of building earthquake responses that are available in the CESMD strong motion database and b) identifying the dynamic characteristics and the amplification effects of nonstructural components during a full-scale building shake table test program. Key findings from this study thus far are summarized as follows:

1. Component amplification effects are not well correlated with the damping ratios of their supporting structures.
2. The vertical distribution profiles of the peak component amplification factors of the first and second modes clearly demonstrate that the component amplification factor is a function of the specific building mode shape and the relative height. This observation corroborates a number of prior studies.
3. According to a limited set of recorded nonstructural seismic responses (five non-rigid components), it appears too conservative to assume an equivalent damping ratio of 2% for nonstructural components during earthquake loads, and in fact in the present study a damping ratio of 5% may be considered as the lower bound value, although some components may attain values as large as 10%.

4. The component amplification effects are highly dependent on the dynamic characteristics of the nonstructural components. The nonstructural components that underwent the largest amplification effects were those with their natural frequencies close to that of a building vibration mode and with smaller damping ratios. The measured amplification factors of these components ranged between 2 and 3 during the earthquake tests.

It is noted that the recorded building responses data analysis currently focuses on the steel moment frame buildings. Investigation of the recorded earthquake responses of the remaining building groups (reinforced concrete shear wall, reinforced concrete moment frame, braced steel frame) is ongoing. The effects of different lateral structural systems on the component amplification effects will be discussed in detail and the results will be included in the final project report.

Acknowledgments

The study presented in this paper is part of a research project funded by the Department of Conservation for the California Strong Motion Instrumentation Program (CSMIP) data interpretation project, agreement No. 1017-564. The helpful suggestions of Dr. Eduardo Miranda, Brett Lizundia, Daniel Swensen, and other members of the SMIAC Subcommittee are greatly appreciated. In addition, the input of John Gillengerten and John Silva during this work is appreciated. The nonstructural component test data was provided by the BNCS experimental program, with its primary support through the National Science Foundation. The BNCS project was a collaboration among four academic institutions (University of California, San Diego; San Diego State University; Howard University; and Worcester Polytechnic Institute), four government or granting agencies (National Science Foundation grant CMMI-0936505, the Englekirk Advisory Board, the Charles Pankow Foundation, and the California Seismic Safety Commission), more than 40 industry partners, and two oversight committees. Many individuals contributed to the overall effort of the BNCS project and the authors acknowledge their support. Opinions and findings of this study are of the authors and do not necessarily reflect those of the sponsors or various partners.

References

Alonso-Rodríguez, A., and Miranda, E. (2016). “Dynamic behavior of buildings with non-uniform stiffness along their height assessed through coupled flexural and shear beams.” *Bulletin of Earthquake Engineering*, *14*(12), 3463-3483.

ASCE (2010). *Minimum Design Loads and Associated Criteria for Buildings and Other Structures*, ASCE/SEI 7-10, Structural Engineering Institute of American Society of Civil Engineers, Reston, Virginia.

ASCE (2016). *Minimum Design Loads and Associated Criteria for Buildings and Other Structures*, ASCE/SEI 7-16, Structural Engineering Institute of American Society of Civil Engineers, Reston, Virginia.

Applied Technology Council (ATC). (1978). “Tentative provisions for the development of seismic regulations for buildings.” *ATC Rep. No. 3-06*, Palo Alto, CA.

Building Seismic Safety Council (BSSC). (1995). *NEHRP recommended provisions for the development of seismic regulations for new buildings*, 1994 Ed., *FEMA 222A*, Federal Emergency Management Agency, Washington, D.C.

Building Seismic Safety Council (BSSC). (1998). *NEHRP recommended provisions for the development of seismic regulations for new buildings*, 1997 Ed., Part 1: Provisions, *FEMA 302*, Federal Emergency Management Agency, Washington, D.C.

CEN (2004). *Eurocode 8: design of structures for earthquake resistance – Part 1: general rules, seismic actions and rules for buildings.* EN 1998-1. Brussels, Belgium.

Chen, M.C., Pantoli, E., Wang, X., Astroza, R., Ebrahimian, H., Mintz, S., Hutchinson, T., Conte, J., Restrepo, J., Meacham, B., Kim, J., and Park, H., 2013a. *BNCS Report #1: Full-scale structural and nonstructural building system performance during earthquakes and post-earthquake fire - specimen design, construction and test protocol.* Report No. SSRP 13/9. University of California San Diego, La Jolla, CA.

Chen, M.C., Pantoli, E., Wang, X., Astroza, R., Ebrahimian, H., Hutchinson, T.C., Conte, J.P., Restrepo, J.I., Marin, C., Walsh, K.D. and Bachman, R.E. (2016). "Full-scale structural and nonstructural building system performance during earthquakes: Part I–Specimen description, test protocol, and structural response." *Earthquake Spectra*, *32*(2), 737-770.

Cruz, C., and Miranda, E. (2016). "Evaluation of damping ratios for the seismic analysis of tall buildings." *ASCE Journal of Structural Engineering*, 143(1), 04016144.

Cruz, C., and Miranda, E. (2019). "Reliability of damping ratios inferred from the seismic response of buildings." *Engineering Structures*, 184, 355-368.

Drake, R.M. and Bachman, R.E. (1996). "NEHRP provisions for 1994 for nonstructural components." *Journal of Architectural Engineering*, 2(1), 26–31.

Fathali, S., and Lizundia, B. (2011). "Evaluation of current seismic design equations for nonstructural components in tall buildings using strong motion records," *The Structural Design of Tall and Special Buildings*, Vol. 20, No. S1, pp. 30-46.

FEMA E-74 (2012). *Reducing the Risks of Nonstructural Earthquake Damage — A Practical Guide.* Federal Emergency Management Agency, Washington, DC.

Hutchinson, T., Restrepo, J., Conte, J., Pantoli, E., Chen, M., Wang, X., Astroza, R., and Ebrahimian, H. (2014). Shake table testing of a five story building outfitted with NCSs (BNCS project). *Network for Earthquake Engineering Simulation (distributor), Dataset, DOI*, *10*, D38W38349.

Kazantzi, A., Vamvatsikos, D., and Miranda, E. (2018). "The effect of yielding on the seismic demands of nonstructural elements," *Proceedings of the 16th European Conference on Earthquake Engineering*, Thessaloniki, Greece.

Lizundia, B. (2019). "Proposed nonstructural seismic design force equations." *Proc., 2019 SEAOC Convention,* Squaw Creek, CA.

NIST (2017). *Seismic Analysis, Design, and Installation of Nonstructural Components and Systems – Background and Recommendations for Future Work*, NIST GCR 17-917-44, National Institute of Standards and Technology, Gaithersburg, Maryland.

NIST (2018). *Recommendations for Improved Seismic Performance of Nonstructural Components*, NIST GCR 18-917-43, National Institute of Standards and Technology, Gaithersburg, Maryland.

NZS1170.5 (2004). *Structural Design Actions Part 5: Earthquake Actions – New Zealand*. Standards Council of New Zealand, Wellington, New Zealand.

Pantoli, E., Chen, M.C., Wang, X., Astroza, R., Ebrahimian, H., Mintz, S., Hutchinson, T., Conte, J., Restrepo, J., Meacham, B., Kim, J., and Park, H., 2013a. *BNCS Report #2: Full-scale structural and nonstructural building system performance during earthquakes and post-earthquake fire - test results.* Report No.SSRP 13/10. University of California San Diego, La Jolla, CA.

Pantoli, E., Chen, M.C., Wang, X., Astroza, R., Ebrahimian, H., Hutchinson, T.C., Conte, J.P., Restrepo, J.I., Marin, C., Walsh, K.D. and Bachman, R.E. (2016). "Full-scale structural and nonstructural building system performance during earthquakes: Part II–NCS damage states." *Earthquake Spectra*, *32*(2), 771-794.

Taghavi, S. and Miranda, E. (2003). *Response assessment of nonstructural building elements*. Report No. PEER-2003/05, Pacific Earthquake Engineering Research Center, Berkeley, CA.

Van Overschee, P., and De Moor, B. (1996). *Subspace system identification for linear systems.* Kluwer Academic Publishers, Boston, MA.

Watkins, D., Chui, L., Hutchinson, T., and Hoehler M. (2010). *Survey and Characterization of Floor and Wall Mounted Mechanical and Electrical Equipment in Buildings*, Report No. SSRP-2009/11, Department of Structural Engineering, University of California, San Diego.